



Dual polarization Fourier transform processor using geometric-phase lenses

PASCUALA GARCÍA-MARTÍNEZ^{1,*}  AND IGNACIO MORENO^{2,3} 

¹Departamento de Óptica y de Optometría y Ciencias de la Visión, Facultad de Física, Universitat de València, 46100 Burjassot, Spain

²Instituto de Bioingeniería, Universidad Miguel Hernández de Elche, 03202 Elche, Spain

³Departamento de Ciencia de Materiales, Óptica y Tecnología Electrónica, Universidad Miguel Hernández de Elche, 03202 Elche, Spain

*pascuala.garcia@uv.es

Abstract: This work presents a novel optical system for polarization image processing using geometric-phase (Pancharatnam-Berry) lenses. Such lenses are half-wave plates where the orientation of the fast (slow) axis follows a quadratic relation with the radial coordinate, and they present the same focal length but opposite sign for left and right circular polarizations. Therefore, they split an input collimated beam in a converging beam and a diverging beam with opposite circular polarizations. This coaxial polarization selectivity introduces a new degree of freedom in optical processing systems and makes it interesting for imaging and filtering applications that require polarization sensitivity. Here we profit from these properties to build an optical Fourier filter system with polarization sensitivity. A telescopic system is used to have access to two real Fourier transform planes, one for each circular polarization. A second symmetric optical system is used to recombine the two beams onto a single final image. As a result, polarization sensitive optical Fourier filtering can be applied, as demonstrated with simple bandpass filters.

© 2023 Optica Publishing Group under the terms of the [Optica Open Access Publishing Agreement](#)

1. Introduction

Optical Fourier transform filtering is a classical topic in Fourier optics [1]. The standard $4f$ system uses a first converging lens to obtain in its back focal plane the Fourier transform (FT) spectrum of an input object located in the front focal plane. This FT plane is real (non-virtual) and a physical filter aperture can be placed in this plane. A second converging lens is placed such that its front focal plane coincides with the FT plane. It produces a second Fourier transform of the filtered field, and the filtered image is obtained in its back focal plane.

Recently there has been a great interest in developing geometric-phase diffractive optical elements (GP-DOE) [2,3], also known as diffractive waveplates [4] or Pancharatnam-Berry phase optical elements [5]. Such elements enable realization of optical components (lenses, prisms, gratings, spiral phase plates, etc.) by patterning the optical axis orientation in the plane of thin anisotropic films. They are typically produced either with metamaterials [6] or with liquid-crystal (LC) materials [7]. Because of their high diffraction efficiency and polarization sensitivity, these functional planar optical elements have been implemented as diffraction gratings [7,8], lenses [9–11], axicons [7,12], vortex wave plates [13,14], and other more complex optical elements leading to fields named as polarization digital holography [7] or polarization diffractive optics [15].

The original GP-DOEs are ideally half-wave retarders (HWR) where the angle of the fast (or slow) axis follows a given spatial pattern $\alpha(\mathbf{r})$, where $\mathbf{r} = (x, y)$ denotes the spatial coordinate in the DOE plane. When the GP-DOE is illuminated with right circularly polarization (RCP), the output beam becomes left circularly polarized (LCP) and gains a phase $\phi_L(\mathbf{r}) = 2\alpha(\mathbf{r})$. On the contrary, when illuminated with LCP, the output becomes RCP and the opposite phase $\phi_R(\mathbf{r}) = -2\alpha(\mathbf{r})$ is acquired. More complex designs involve not only controlling the orientation of

the spatial retarder at each position, but also an additional spatially varying phase, thus allowing to encode two independent phase functions onto the two circular polarizations. However, this introduces fabrication complexity, and this is usually achieved better with metamaterial elements. In this work we consider standard liquid-crystal GP lenses, since they are commercially available.

A growing number of imaging techniques and applications make use of polarization of light [16]. This is becoming specially interesting in biological samples [17], and the application of polarization DOE enable new tools to make polarimetric systems more compact and efficient than classical systems [18]. The miniaturization trend demanded by emerging technologies for smartphones, wearables, automotive and virtual reality, is pushing the research towards flat and lightweight DOE devices that perform their conventional counterpart [19].

GP lenses provide two back focal planes, one real and one virtual, one for each circular polarization. Thus, in general, they split the light from a given object plane into two circularly polarized beams that provide two different image planes. Some works have presented combinations of GP lenses to provide a unique polarization independent image plane [20]. In this work, on the contrary, we exploit this polarization splitting property to implement a polarization Fourier transform filtering optical system. We use a telescopic system to image the two back focal planes provided by the GP lens onto two real foci, both with the same magnification [21]. The attractive aspect of this system is that it provides two axially displaced real (non-virtual) Fourier transform planes, where a different filtering operation can be applied. Then a second Fourier transform is achieved with a second telescopic system and a second GP lens, to merge the two filtered polarized images. As a result, a unique image plane is obtained but a polarization sensitive Fourier transform filtering can be applied. An experimental proof-of-concept is provided with some basic filtering operations.

The paper is organized as follows: after this introduction, Section 2 describes the principles of GP lenses, and some results of their focalization properties and dependence on the polarization. Section 3 shows the dual Fourier transform properties of these lenses. Then Section 4 presents the optical processor based on the manipulation of the two Fourier planes with different polarization created by the GP lenses, as well as providing some image processing experimental results. Conclusions are given in Section 5.

2. Geometric phase lenses: principles and focalization results

2.1. Principles

Figure 1 shows the principle of operation of the GP lens (GPL). Here the orientation of the LC pattern follows the function $\alpha(\mathbf{r}) = \pi r^2 / 2\lambda f_{GPL}$ where $r = \sqrt{x^2 + y^2}$ is the radial coordinate in the lens plane, f_{GPL} denotes GPL focal length and λ is the operating wavelength. According to the principles of GP-DOEs, this element acts on input LCP light as a converging lens and for input RCP light as a diverging lens, and additionally transforms RCP into LCP and vice versa. Therefore, if the lens is illuminated with a collimated linearly polarized beam, it is split in two beams, one RCP converging beam focusing at a real image focus F_R located a distance $+f_{GPL}$ after the lens, and one LCP diverging beam, diverging from a virtual image focus F_L located a distance $-f_{GPL}$ before the lens (Fig. 1(a)).

One interesting property of GPLs that we use in this work is that the polarization circular components (RCP and LCP) that is focused or diverged can be switched simply by reversing the orientation of the lens. This is illustrated in Figs. 1(a) and 1(b) where the darker green line indicates in each case one of the two surfaces of the lens. We assume the lens illuminated with a collimated linearly polarized beam so both, the converging and the diverging beams have the same weight. In Fig. 1(a) the RCP component is converging while the LCP component is diverging. In Fig. 1(b), after reversal of the lens, the focused beam is now LCP while the diverging beam is RCP. Figures 1(c) and 1(d) sketch the spatial distribution of the LC director in each case,

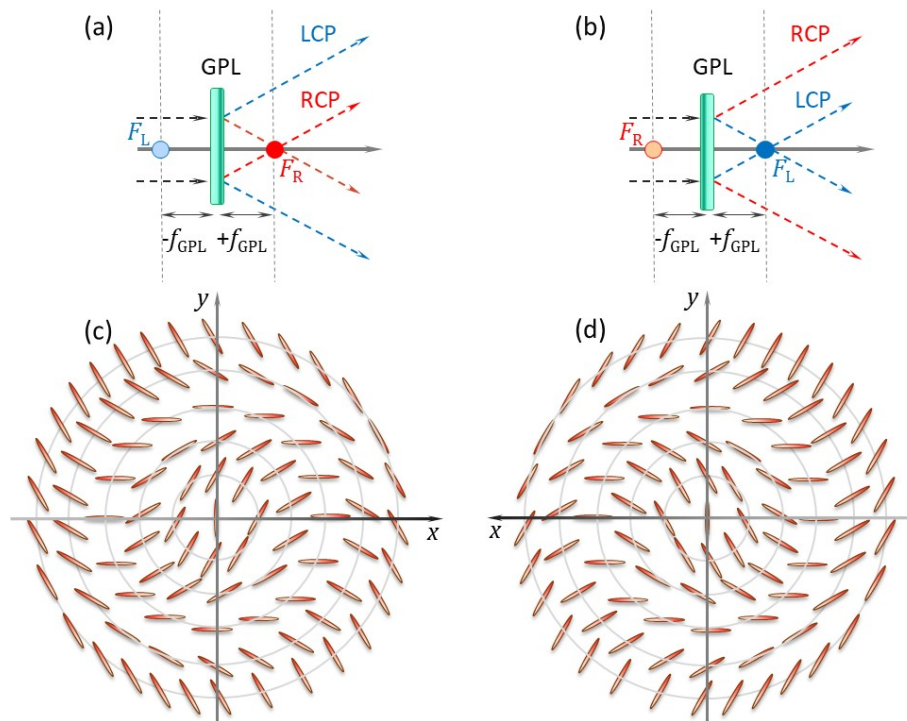


Fig. 1. (a) Polarization directed feature of a geometric-phase lens. (b) Equivalent feature when the lens is reversed. In both cases the collimated input beam is assumed linearly polarized. (c) Illustration of the LC director spatial distribution $\alpha(\mathbf{r})$ for the geometric-phase lens. (d) Equivalent distribution after flip around the y -axis, showing that the distribution becomes $-\alpha(\mathbf{r})$.

which helps to understand why this effect occurs. In Fig. 1(c) we draw the distribution of the LC director axis in the GPL, which follows a pattern $\alpha(\mathbf{r})$ proportional to r^2 . The LC director rotates clockwise as the radial coordinate increases. Figure 1(d) shows the equivalent drawing but where a horizontal flip (flip around the vertical y -axis) has been performed. Note how this flip changes the sense of rotation of the LC distribution, which now rotates anticlockwise with the radial coordinate. Therefore, the spatial distribution in Fig. 1(d) is now $-\alpha(\mathbf{r})$ compared to that in Fig. 1(c). This explains why now the polarization states that become convergent/divergent have switched. Symmetric conventional refractive or diffractive lenses do not change focusing properties when the lens is flipped, but in these GPLs this fact is crucial and must be taken into account as we show next in the Fourier processor described in Section 4.

2.2. Focalization results

We employ GPLs acquired from Edmund Optics, there known as polarization directed flat lenses. These are polymerized liquid-crystal thin-films, approximately 0.45 mm thick, with an effective area of $2.5 \times 2.5 \text{ cm}^2$, and a nominal focal length of $f_{\text{GPL}} = 100 \text{ mm}$, useful in the visible range [22]. We use a 632.8 nm wavelength linearly polarized He-Ne laser. The beam is spatially filtered and collimated. A quarter-wave plate mounted on a rotatable mount is placed in the system so the beam can be transformed into circularly polarized before being directed to a GPL. A CCD camera (Basler scA1300-200um) is placed on the back focal plane of the GPL.

Figure 2 shows experimental results. In this figure we keep the input intensity constant, but we deliberately overexpose the camera images so the two beams can be clearly visible. In Fig. 2(a) the GPL has been removed, so the input collimated beam directly impinges on the camera. In Fig. 2(b) the input beam is linearly polarized, and we observe the decomposition of the input light in two beams: a converging beam which is focused on the camera, and a diverging beam, which appears on the plane with a size bigger than the original beam in Fig. 2(a). Figures 2(c) and 2(d) show the captures when the GPL is illuminated with LCP and RCP states respectively. In the first case, only the converging focused beam is present, while in the second case only the diverging beam is present (a very weak converging beam is still observed due to a non-perfect full polarization conversion in the GPL).

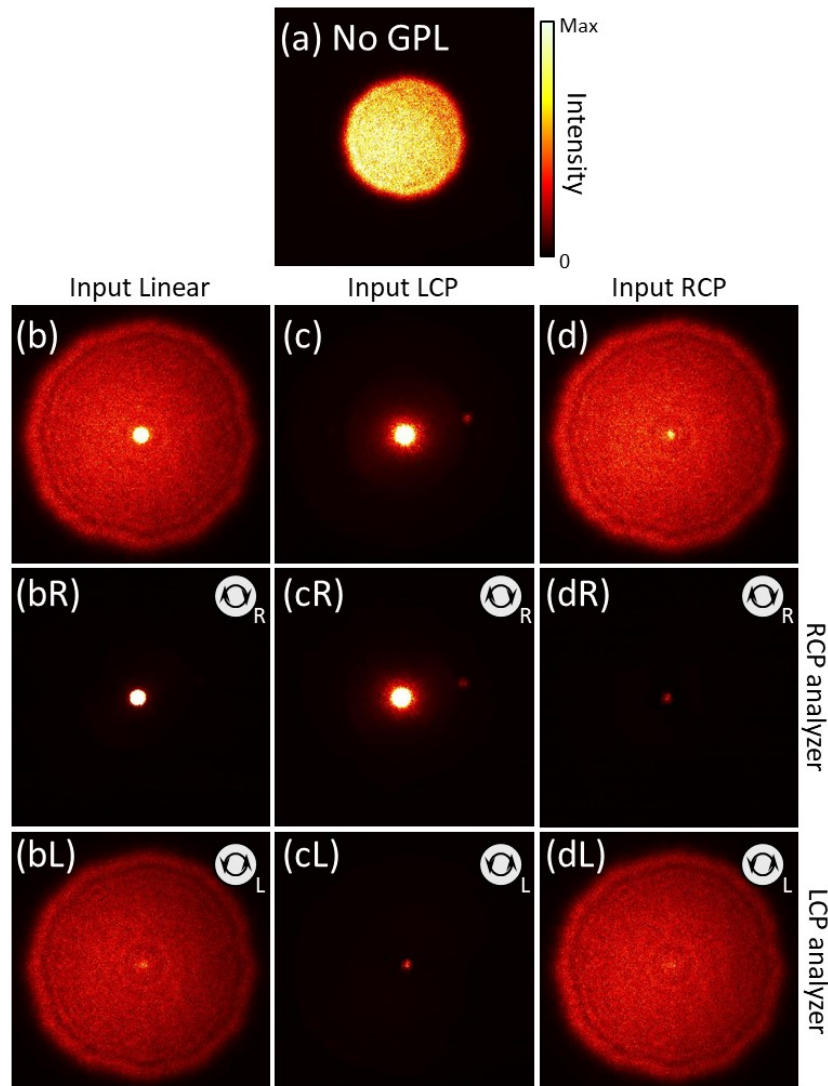


Fig. 2. Experimental captures of the laser beam when (a) without GPL, (b) with GPL illuminated with linearly polarization, (c) with GPL illuminated with LC polarization and (d) with GPL illuminated with RC polarization.

Figures 2(bR), 2(cR) and 2(dR) show the corresponding images when a RCP polarizer analyzer (composed by a quarter-wave plate and a linear analyzer) is placed before the camera. Equivalent results shown in Figs. 2(bL), 2(cL) and 2(dL) correspond to using a LCP analyzer. These results verify that, for this selected orientation of the GPL, the converging beam is RCP, and it is generated when the input beam is LCP, while the diverging beam is LCP and generated when the input beam is RCP. Finally, we verified that flipping the lens (like in Fig. 1(d)) interchanges the circular polarization component that converges / diverges.

3. Optical Fourier transform with geometric-phase lens

One of the more advanced topics in image processing has to do with the concept of Fourier transform (FT) [1]. A $2f$ lens system is the simplest way to perform a FT. When an object is placed in the front focal plane and it is illuminated with collimated beam, the exact FT is obtained in its back focal plane [1]. If the object is not placed in the lens front focal plane, the FT is still obtained in the back focal plane but multiplied by a quadratic phase term. Here we exploit the properties of the GPL to perform the optical FT. With the classical $2f$ scheme in mind, the GPL is suitable to perform optical FT for circularly polarized light component that is focused (convergent lens). The diverging lens produces a virtual FT in its virtual back focal plane, but not being a real field is not accessible. However, this virtual plane can be imaged onto a real image with the aid of another lens.

A dual circular polarization bifocal lens with two real foci could be created with a lens doublet that combines the GPL with another attached standard converging glass lens with greater optical power. If $f_L < f_{GPL}$, where f_L indicates the glass lens focal length, both circular polarization components will experience converging lenses, thus producing two different real FT fields at two different axial planes (Fig. 3(a)). In practice there is a separation d between the GPL and the standard lens, so the doublet will behave as a bifocal lens with focal lengths f_{\pm}

$$f_{\pm} = \frac{\pm f_{GPL} f_L}{f_L \pm f_{GPL} - d} \quad (1)$$

where subindex \pm in f_{\pm} stands for the doublet focal lengths for the positive and for the negative value of f_{GPL} respectively, i.e. where the RCP and LCP beams get focused. By properly selecting f_L and d the two FT planes can be made real, so filtering operations can be made on each of them. However, since the focal lengths f_+ and f_- are different for each focus, so does the scale of the FT transform.

Here, instead, we are more interested in obtaining two FT planes with the same scale, so the filtering operations could be applied with the same kind of filters. To achieve this situation, the GPL can be combined with a telescopic system (telecentric lens), as shown in Fig. 3(b), formed by two converging lenses L_1 and L_2 , so the back focal plane of L_1 coincides with the front focal plane of L_2 . One relevant property of telecentric lenses is that they produce images of objects located at different distances with the same magnification. Therefore, we can use it to produce two real images of the two FT planes provided by the GPL. Here we built a simple such system by combining two converging lenses L_1 and L_2 separated a distance $f_1 + f_2$. If the virtual focal plane of the GPL (indicated as the blue dot F_{L1} , in Fig. 3(b)) is closer to L_1 than its focal length f_1 , the telescope produces two real foci (F_{L2} and F_{R2}) behind lens L_2 , which are real images of the GPL foci (F_{L1} and F_{R1}), and both with the same magnification.

If the object plane is located before the GP lens, these two axially separated planes will provide two FT fields, one for each circular polarization component. The back principal plane for the complete system (GPL – telescope lens system) lies exactly in between, where the telescope gives the image of the GPL, so the two focal lengths for the complete system are now $f_+ = +f_{GPL}$ and $f_- = -f_{GPL}$. A more detailed description of the imaging properties of the combination of a GP lens and the telescope was presented in [21].

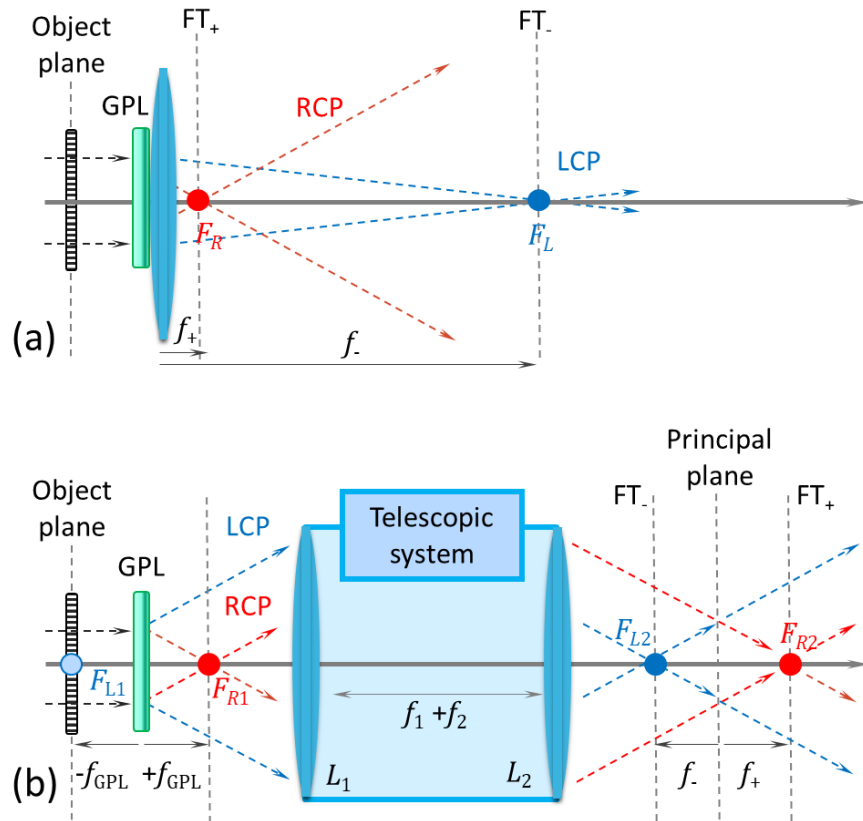


Fig. 3. Two possible optical systems to obtain dual polarization FT with GPL: (a) Doublet lens made of the GPL and a convergent lens with more power. (b) GP lens followed by a telescopic system.

Figure 4 shows experimental results that confirm these properties. First, we combined the GPL with a glass lens of shorter focal length, to achieve two axially separated real foci (system in Fig. 3(a)). In this case we used a focal length of $f_L = +75$ mm and the lens was placed behind the GPL a distance approximately $d = 50$ mm. Therefore, since $f_{GPL} = 100$ mm, from Eq. (1) the GPL - glass lens doublet has two focal lengths $f_+ = 60$ mm and $f_- = 100$ mm respectively. Note that in this situation f_- takes the same value as f_{GPL} .

A Fourier transform computer-generated hologram (CGH) was placed at the object plane before the GPL, at a distance approximately its focal length f_{GPL} . Figures 4(a) and 4(b) show the captures of a CCD detector, placed behind the lens doublet at two different axial distances where the CGH reconstruction is focused, i.e., the two real FT planes for LCP and for RCP polarizations, respectively. In each plane the CGH reconstruction is recovered (in this case the skull pattern). In these results, the system is illuminated with linearly polarized light, so the input beam is split by the GPL in the two (converging and diverging) beams with equal intensity. The results in Fig. 4 show that both FT patterns appear with the same orientation but with a different scale. The pattern closest to the lens (Fig. 4(a)) is smaller than the one focused further away (Fig. 4(b)). These two FT-CGH reconstructions are circularly polarized, each one with opposite helicity. The smaller CGH reconstruction (Fig. 4(a)) is RCP polarized, while the larger one (Fig. 4(b)) is LCP polarized. The combination with the glass lens makes the RCP light focus closer while the LCP light focus further away. Since the size of the FT scales with the focal length of the doublet, this

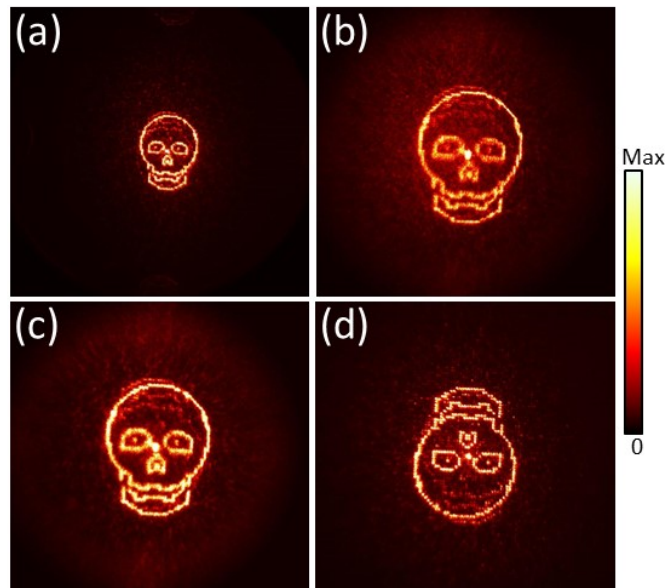


Fig. 4. Experimental reconstruction of a CGH at the two real FT planes obtained with (a),(b) GPL with attached converging lens (system in Fig. 3(a)). (c),(d) GP lens with telescope system (system in Fig. 3(b)). In both cases the input beam is linearly polarized.

explains why the size of the RCP focalization appears 0.6 times the size of the LCP focalization, in agreement with the ratio of focal lengths f_+/f_- .

Figures 4(c) and 4(d) show equivalent results but now the GPL is combined with the telescopic system, made of two glass lenses both with the same focal length of $f_1 = f_2 = 100$ mm, so the telescope magnification is unity, and scale of the FT is the same as in the previous case. In this case we again obtain two CGH reconstructions at two different axial planes behind the telescope. The one closest to the telescope (Fig. 4(c)) appears upright, while the one further away appears with the same scale, but inverted. The reason is that the telescope produces a -1 magnification, therefore inverting the CGH reconstruction. In Fig. 4(c) this inversion is compensated by the inversion produced by the negative focal length of the GP lens diverging part. Like in the previous case, the two CGH reconstructions are circularly polarized with opposite helicity. In each reconstruction, the plane the opposite circular polarization appears as some weak unfocused background.

4. Dual polarization Fourier transform filtering

4.1. Optical setup

A classical optical scheme of huge importance and utility in many applications of coherent optics is the so-called $4f$ system, where the first lens with a focal length of f performs a first FT on the wavefront; the second, with a focal length of f , collects the Fourier spectrum and performs another FT. Ideally, the $4f$ system has two equal lenses spaced by twice their focal length. For image processing and filtering, a hologram or a mask is placed in the Fourier plane (back focal plane of first lens) in order to manipulate the Fourier spectrum.

Different optical processors have exploited filtering operations based on modifying the state of polarization in the FT plane [23], with special interest for the generation of complex vector beams [24,25]. In Ref. [26] the authors proposed a combination of an interferometer and a $4f$ spatial polarization filtering system using LED illumination to reduce coherent noise. The

novelty of our work here is the design of the optical FT processor using two FT systems like in Fig. 3(b). The first dual polarization FT demonstrated in Section 3 provides access to two axially displaced FT planes having opposite circular polarizations. Therefore, we can apply two independent FT filters to each polarization. Then, a second FT system provides a recombination of the two filtered beams to obtain a final image. Figure 5 shows a scheme of the complete optical system. A second telescope system is added after the two FT filters. It provides two images (F_{L3} and F_{R3}) with the same magnification of the FT planes at two output planes. In these telescope systems we use two lenses of focal lengths 100 mm focal length to build the second telescope. This way a minus unit magnification is obtained at each step, and the distance between the output foci pair (F_{L3} and F_{R3}) is the same as that of the input foci pair (F_{L1} and F_{R1}). Thus, a second GP lens (GPL2) with the same focal length as the input one (GPL1) can be used to recombine the two filtered beams. A key point is to orient this second GP lens flipped with respect to the first one, as we explained in Fig. 1. Note that the virtual focus of GPL1 (F_{L1}) is now imaged closer to the second telescope (F_{L3}) than the image of real focus (F_{R3}).

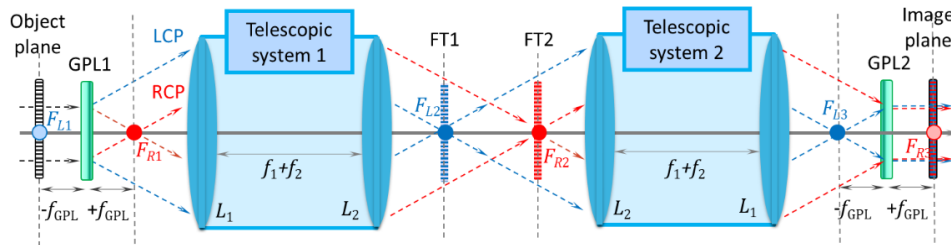


Fig. 5. Scheme of the dual circular polarization FT processor setup.

The input object is placed before the first GPL. Using the telescope system, the two real FT planes are accessible and different masks and pupils can be placed to make different image processing operations for the RCP and LCP polarizations separately. To obtain a single output plane, we reproduce the same system but symmetrical having another telescopic system and a final GPL that is placed in a reverse mode. This way, the concatenation of the two telescopes provides a final image with the same magnification for the two circular polarization components.

4.2. Experimental results

Figure 6 shows some experimental results. Here we use a binary amplitude object pattern consisting of the number “2”. In order to see the two images in the final output plane, the second GPL that recombines the two beams is slightly shifted laterally, so the two images do not overlap. In these results no filtering mask is placed in the two Fourier planes, so the “2” pattern is recovered. When we used input linear polarization (Fig. 6(a)), the two images of the input object are obtained, one RCP and the other one LCP. On the contrary if the system is illuminated with LCP or RCP, one single image is obtained. Figures 6(b) and 6(c) show these situations. We remind that each GPL produces an inversion of the helicity of the circular polarization, so the “2” image in Fig. 6(b) is LCP while the “2” image in Fig. 6(c) is RCP.

To independently modify the FT fields for the two polarizations, we need to apply filters in the FT planes that affect only one polarization. This could be achieved by transforming the circular polarizations into two orthogonal linear polarizations (with a quarter-wave plate) and using liquid-crystal (LC) SLM technology. Since the linear polarization component perpendicular to the LC director is unaffected by the LC-SLM, the filter only affects the orthogonal polarization component. Therefore, either using two SLMs or with two passages through one SLM with a polarization switch in between [27], independent polarization filtering operations could be

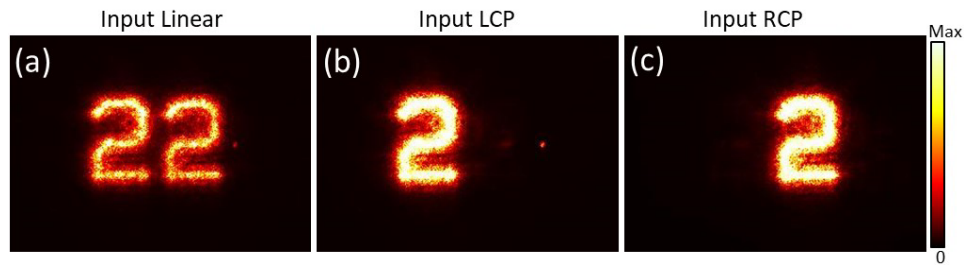


Fig. 6. Experimental results of the final image plane when an input “2” binary amplitude object is used. (a) Input beam with linear polarization. (b) Input beam LCP. (c) Input beam RCP.

applied on each plane. A second quarter-wave plate would transform the orthogonal linear polarizations onto circular polarizations in the second FT stage.

In this work, however, we show a much simpler proof-of-concept using very simple filtering operations with amplitude filters. Figure 7 shows the filters tested and the corresponding experimental results captured in the final output image. In these experiments we have illuminated the system with linearly polarized light, so the two images are present in the final plane. We used simple high-pass filters where the center of the FT is blocked with a very narrow dark line or a very small dot. Such filters, removing the low frequencies of the FT, produce an edge enhancement at the output image. Since we have available two FT planes, we have tested placing the filters at these two planes.

For instance, Fig. 7(a) and Fig. 7(b) show the results when the filter is a narrow vertical line, which is placed either in FT1 plane or in FT2 plane, respectively. In the first case, when the vertical line filter is placed at FT1 plane, where the LCP beam is focused, we observe the filtering of the image on the right. On the contrary, the image on the left is not being affected since the RCP beam FT is highly defocused in the plane FT1 where the filter is placed. When the same filter is moved to the FT2 plane, the situation is reversed, and now is the “2” image on the left the one that is filtered with the image on the right is unaffected. Note how in these results the edge enhancement at the filtered image is produced at the vertical borders, while the horizontal borders tend to disappear. The reason is that the vertical line filter completely removes vertical spatial frequencies, while leave the horizontal high frequencies.

The situation changes when a horizontal line filter is used, as shown in Fig. 7(c) and Fig. 7(d). Again, like in the previous results, one image remains unaltered while the other is filtered, since the filter is placed either in FT1 or in FT2 planes, respectively. But now the filtered image shows the edge enhancement in the horizontal borders, while the vertical borders are those that are eliminated. In Fig. 7(e) we consider the situation where the horizontal line filter is placed in FT1 plane, while a vertical line filter is placed at FT2 plane. Now both images are filtered, but the edge enhancement is produced in orthogonal directions on each image. Finally, in Fig. 7(f) we show the case when we use a dot filter in FT1 plane, while FT2 plane is unfiltered. Now the filtering is produced equally in all directions and therefore the edge-enhancement is produced both in vertical and horizontal borders of the filtered image.

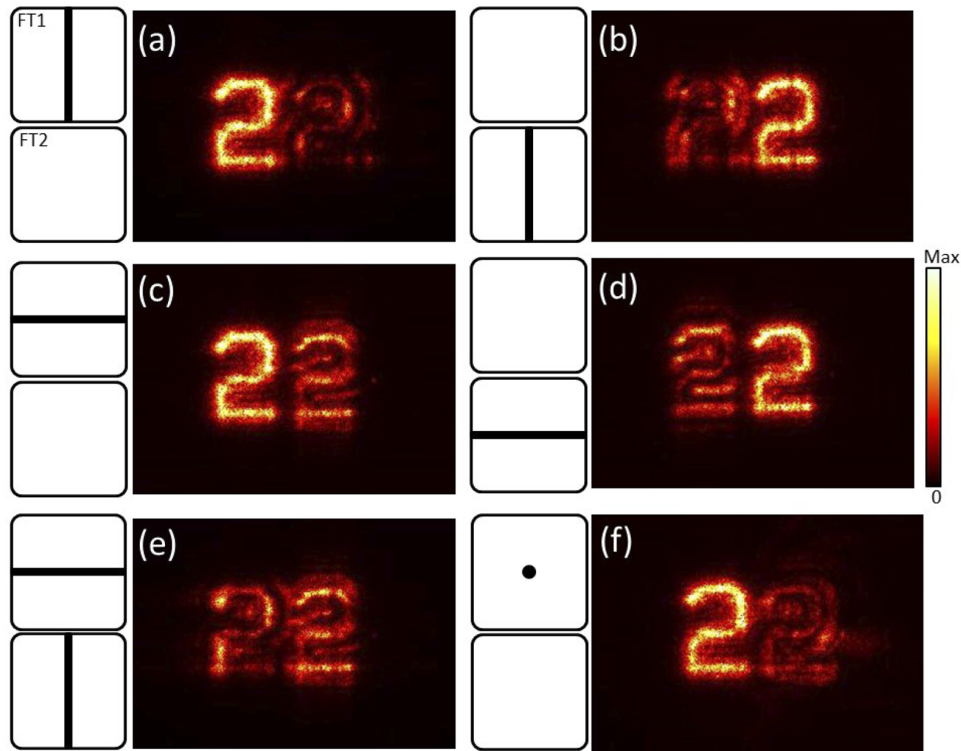


Fig. 7. Experimental results of the dual polarization FT filtering with binary amplitude high-pass filters. (a) Vertical line filter at FT1 plane. (b) Vertical line filter at FT2 plane. (c) Horizontal line filter at FT1 plane. (d) Horizontal line filter at FT2 plane. (e) Horizontal line filter at FT1 plane and vertical line filter at FT2 plane. (f) Dot filter at FT1 plane.

5. Conclusions

In conclusion, we have proposed a new dual polarization Fourier transform processor based on the use of GP lenses. We exploit the bifocal property of such lenses, with two focal lengths, one positive and one negative, with the same magnitude, to obtain two axially separated Fourier transforms of the same object, each with different polarization, one RCP and one LCP. However, one of these two FT planes is virtual, since corresponds to a negative focal length. With the aid of a telescope system, we showed that the two axially shifted Fourier transforms planes can be made real, so physical optical FT filters can be placed to alter the FT spectrum. These two Fourier transforms have the same scale although they are inverted. This is opposed to the situation where the real FT planes are obtained by adding a convergent lens with greater power than the GPL, that provides the same orientation of the FT, but different scaling.

Then, a second FT system is completed to perform a with another telescope and another GPL. A key aspect to recombine the two beams is noting that the GPL can be flipped to invert the polarization component for which it acts as convergent or divergent. The complete system thus provides two FT planes with opposite circular polarizations to independently modify the spectrum. Experimental proof-of-concept has been presented with simple amplitude filters, that confirm the usefulness of the system. Future applications of polarization sensitivity filtering applied to biological samples could be of great interest.

Funding. Conselleria de Innovación, Universidades, Ciencia y Sociedad Digital, Generalitat Valenciana (ref. CIAICO/2021/276); Ministerio de Ciencia e Innovación (ref.: PID2021-126509OB-C22).

Disclosures. The authors declare no conflicts of interest.

Data availability. Data underlying the results presented in this paper are not publicly available at this time but may be obtained from the authors upon reasonable request.

References

1. J. W. Goodman, *Introduction to Fourier Optics*, 3rd ed., Roberts & Company Publishers, (2004).
2. C. P. Jisha, S. Nolte, and A. Alberucci, "Geometric phase in Optics: From wavefront manipulation to waveguiding," *Laser Photonics Rev.* **15**(10), 2100003 (2021).
3. L. De Sio, D.E Roberts, Z. Liao, S. Nersisyan, O. Uskova, L. Wickboldt, N. Tabiryán, D. M. Steeves, and B. R. Kimball, "Digital polarization holography advancing geometrical phase optics," *Opt. Express* **24**(16), 18297 (2016).
4. S. V. Serak, D. E. Roberts, J.-Y. Hwang, S. R. Nersisyan, N. V. Tabiryán, T. J. Bunning, D. M. Steeves, and B. R. Kimball, "Diffractive waveplate arrays," *J. Opt. Soc. Am. B* **34**(5), B56–B63 (2017).
5. T. Zhan, Y.-H. Lee, G. Tan, J. Xiong, K. Yin, F. Gou, J. Zou, N. Zhang, D. Zhao, J. Yang, S. Liu, and S.-T. Wu, "Pancharatnam–Berry optical elements for head-up and near-eye displays," *J. Opt. Soc. Am. B* **36**(5), D52–D65 (2019).
6. J. P. B. Mueller, N. A. Rubin, R. C. Devlin, B. Groever, and F. Capasso, "Metasurface polarization optics: independent phase control of arbitrary orthogonal states of polarization," *Phys. Rev. Lett.* **118**(11), 113901 (2017).
7. J. Kim, Y. Li, M. N. Miskiewicz, J. Oh, M. W. Kudenov, and M. J. Escuti, "Fabrication of ideal geometric-phase holograms with arbitrary wavefronts," *Optica* **2**(11), 958–964 (2015).
8. K. Gao, C. McGinty, H. Payson, S. Berry, J. Vornehm, V. Finnmeyer, B. Roberts, and P. Bos, "High-efficiency large-angle Pancharatnam phase deflector based on dual-twist design," *Opt. Express* **25**(6), 6283–6293 (2017).
9. M. Khorasaninejad, W. T. Chen, R. C. Devlin, J. Oh, A. Y. Zhu, and F. Capasso, "Metalenses at visible wavelengths: Diffraction-limited focusing and subwavelength resolution imaging," *Science* **352**(6290), 1190–1194 (2016).
10. X. Chen, M. Chen, M. Q. Mehmood, D. Wen, F. Yue, C.-W. Qiu, and S. Zhang, "Longitudinal multifoci metalens for circularly polarized light," *Adv. Opt. Mater.* **3**(9), 1201–1206 (2015).
11. K. Gao, H.-H. Cheng, A. K. Bhowmik, and P. J. Bos, "Thin-film Pancharatnam lens with low f-number and high quality," *Opt. Express* **23**(20), 26086–26094 (2015).
12. M. Fratz, S. Sinzinger, and D. Giel, "Design and fabrication of polarization-holographic elements for laser beam shaping," *Appl. Opt.* **48**(14), 2669–2677 (2009).
13. S. Slussarenko, A. Murauski, T. Du, V. Chigrinov, L. Marrucci, and E. Santamato, "Tunable liquid crystal q-plates with arbitrary topological charge," *Opt. Express* **19**(5), 4085–4090 (2011).
14. W. Ji, C. H. Lee, P. Chen, W. Hu, Y. Ming, L. Zhang, T. H. Lin, V. Chigrinov, and Y. Q. Lu, "Meta-q-plate for complex beam shaping," *Sci. Rep.* **6**(1), 25528 (2016).
15. N. A. Rubin, Z. Shi, and F. Capasso, "Polarization in diffractive optics and metasurfaces," *Adv. Opt. Photonics* **13**(4), 836–970 (2021).
16. S. G. Demos and R. R. Alfano, "Optical polarization imaging," *Appl. Opt.* **36**(1), 150–155 (1997).
17. C. He, H. He, J. Chang, B. Chen, H. Ma, and M. J. Booth, "Polarisation optics for biomedical and clinical applications: a review," *Light: Sci. Appl.* **10**(1), 194 (2021).
18. N. A. Rubin, G. D'Aversa, P. Chevalier, Z. Shi, W. T. Chen, and F. Capasso, "Matrix Fourier optics enables a compact full-Stokes polarization camera," *Science* **365**(6448), eaax1839 (2019).
19. W. T. Chen and F. Capasso, "Will flat optics appear in everyday life anytime soon?" *Appl. Phys. Lett.* **118**(10), 100503 (2021).
20. T. Zhan, J. Xiong, Y.-H. Lee, and S.-T. Wu, "Polarization-independent Pancharatnam–Berry phase lens system," *Opt. Express* **26**(26), 35026–35033 (2018).
21. A. Cofré, A. Vargas, F. A. Torres-Ruiz, M. M. Sánchez-López, and I. Moreno, "Geometrical-phase lens based optical system for the spin-splitting of vector beams," *Opt. Lasers Eng.* **110**, 401–409 (2018).
22. Edmund Optics, Polarization Directed Flat Lenses <https://www.edmundoptics.es/knowledge-center/trending-in-optics/polarization-directed-flat-lenses/>
23. I. Moreno, C. Iemmi, J. Campos, and M. J. Yzuel, "Jones matrix treatment for optical Fourier processors with structured polarization," *Opt. Express* **19**(5), 4583–4594 (2011).
24. H. Chen, J. Hao, B.-F. Zhang, J. Xu, J. Ding, and H.-T. Wang, "Generation of vector beam with space-variant distribution of both polarization and phase," *Opt. Lett.* **36**(16), 3179–3181 (2011).
25. J. A. Davis, I. Moreno, M. M. Sánchez-López, and D. M. Cottrell, "Vector beams generated with a Fourier transform processor with geometric phase grating," *Opt. Eng.* **62**(01), 013104 (2023).
26. R. Guo, B. Yao, P. Gao, J. Min, M. Zhou, J. Han, X. Yu, X. Yu, M. Lei, S. Yan, Y. Yang, D. Dan, and T. Ye, "Off-axis digital holographic microscopy with LED illumination based on polarization filtering," *Appl. Opt.* **52**(34), 8233–8238 (2013).
27. I. Moreno, J. A. Davis, T. Hernandez, D. M. Cottrell, and D. Sand, "Complete polarization control of light from a liquid crystal spatial light modulator," *Opt. Express* **20**(1), 364–376 (2012).